New insight into lunar impact melt mobility from the LRO camera

V. J. Bray,[1] L. L. Tornabene,[1] L. P. Keszthelyi,[2] A. S. McEwen,[1] B. R. Hawke,[3] T. A. Giguere,[3] S. A. Kattenhorn,[4] W. B. Garry,[5] B. Rizk,[1] C. M. Caudill,[1] L. R. Gaddis,[2] and C. H. van der Bogert[6]

Received 12 July 2010; revised 23 September 2010; accepted 30 September 2010; published 13 November 2010.

[1] The Lunar Reconnaissance Orbiter Camera (LROC) is systematically imaging impact melt deposits in and around lunar craters at meter and sub-meter scales. These images reveal that lunar impact melts, although morphologically similar to terrestrial lava flows of similar size, exhibit distinctive features (e.g., erosional channels). Although generated in a single rapid event, the post-impact mobility and morphology of lunar impact melts is surprisingly complex. We present evidence for multi-stage influx of impact melt into flow lobes and crater floor ponds. Our volume and cooling time estimates for the post-emplacement melt movements noted in LROC images suggest that new flows can emerge from melt ponds an extended time period after the impact event. **Citation:** Bray, V. J., et al. (2010), New insight into lunar impact melt mobility from the LRO camera, *Geophys. Res. Lett.*, *37*, L21202, doi:10.1029/2010GL044666.

1. Introduction

[2] Production of melted target material is a fundamental process in hypervelocity impact events. The amount and distribution of impact melt is influenced by many factors including impact velocity, impact angle, and target properties [e.g., *O'Keefe and Ahrens*, 1975; *Pierazzo and Melosh*, 2000; *Kieffer and Simonds*, 1980]. Estimation of impact melt volumes and understanding of post-emplacement melt movement and admixture of rocky debris thus provide context for melt-bearing impact products, and a means to study the impact process itself. As impact products on Earth (and to a lesser extent, Mars) are subject to extensive interaction with volatiles, erosion, and alteration, melt-bearing deposits in fresh lunar craters provide excellent examples of pristine melt product morphology and distribution.

[3] We present examples of 5–100 m scale features of impact melt deposits in three fresh complex lunar craters (Figure S1 and Table S1 of the auxiliary material)[1] revealed by high-resolution (~0.5–2.0 m/pixel) images from the Lunar Reconnaissance Orbiter Narrow Angle Camera (LROC-NAC) [*Robinson et al.*, 2010], and use the morphological characteristics and stratigraphic relationships inferred from these new images to investigate the evolution of melt ponds and flows. The variety of viewing and sun angles now available from LROC images reveal previously unseen characteristics of impact melt, which provide evidence for the highly mobile nature of melt after emplacement.

2. Methods

[4] Fresh Copernican craters that possess distinctive ray patterns (high contrast in both Clementine albedo and color-ratio images) and well-preserved morphology were specifically targeted for LROC-NAC imaging to study the morphology of crater and melt-deposits. Measurements presented in this work were obtained from full-resolution NAC images. Impact melts were identified on the basis of their spatial association with craters, surface cooling fractures, and morphologic flow features (ponding to a level surface, lobate flows and leveed channels, etc. [e.g., *Howard and Wilshire*, 1975]). The "impact melts" presented in this work refer to a mix of melt and solid rock fragments of various shock levels that have been incorporated during melt movement and emplacement.

[5] To estimate cooling times of flows and ponds we used the 1-D numerical model of an infinite half-space losing heat by thermal radiation developed by *Keszthelyi and Denlinger* [1996]. The use of a 1-D model is appropriate because the flows are much thinner than they are wide (e.g., 2–10 m deep and ~445 m across in Figure 4b). We updated the model for lunar surface conditions, assuming no heat loss via atmospheric convection, an ambient temperature of 250 K, and an ultramafic/mafic composition with latent heat and heat capacity relevant to lunar basalt. We explored a parameter space including initial melt temperatures between 1600 K and a super-heated value of 2000 K [*O'Keefe and Ahrens*, 1975], and melt vesicularities of 0–25% as reported for lunar impact melts [*Butler*, 1973]. Cooling time estimates reported here are based on 2000 K melt; different vesicularities and starting temperatures affect estimates by ~20–50%.

3. Observations

3.1. Prolonged Movement of Floor Melt Deposits

[6] Melt deposits on the floors of complex craters are comprised of a mixture of melt and clastic debris, giving the majority of deposits a hummocky appearance (e.g., 'H' in Figure S2). Smoother floor melt deposits tend to occur in

[1]Lunar and Planetary Laboratory, University of Arizona, Tucson, Arizona, USA.
[2]United States Geological Survey, Flagstaff, Arizona, USA.
[3]Hawaii Institute of Geophysics and Planetology, University of Hawaii at Manoa, Honolulu, Hawaii, USA.
[4]Department of Geological Sciences, University of Idaho, Moscow, Idaho, USA.
[5]Center for Earth and Planetary Studies, National Air and Space Museum, Smithsonian Institution, Washington, DC, USA.
[6]Institut für Planetologie, Westfälische Wilhelms-Universität, Münster, Germany.

0094-8276/10/2010GL044666

[1]Auxiliary materials are available in the HTML. doi:10.1029/2010GL044666.

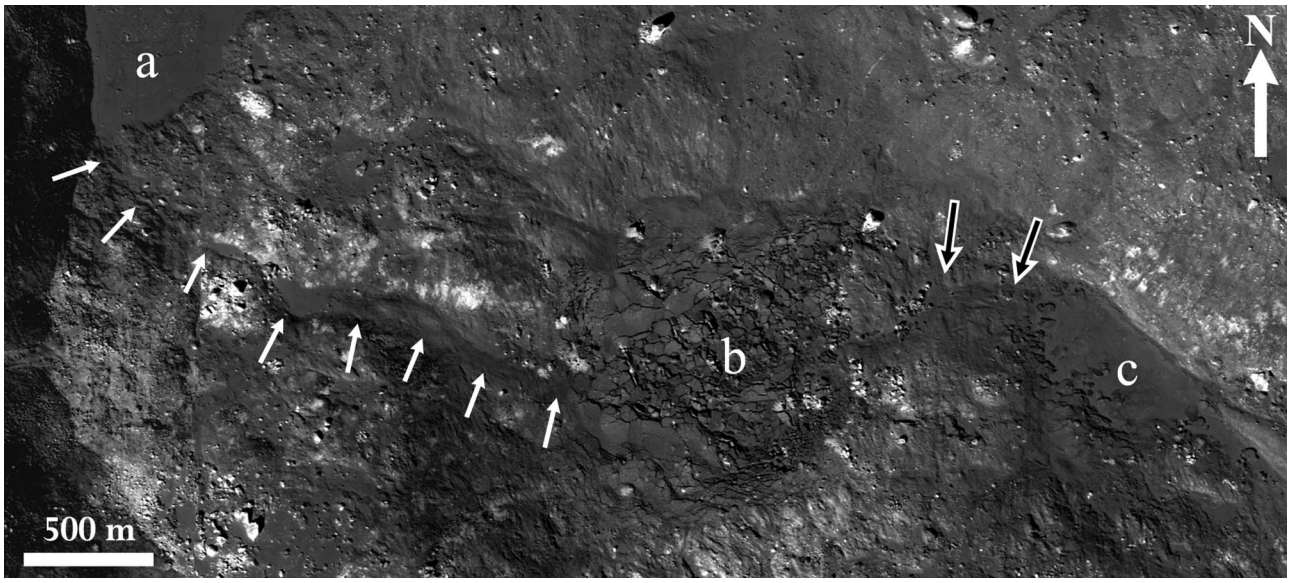

Figure 1. LROC-NAC image M110919730 showing flow between three melt ponds on the floor of Giordano Bruno. The southernmost tip of the smooth impact melt pond in Figure 2a is seen in the upper left corner (pond a). White arrows mark the flow path of melt between ponds a and b, black-in-white arrows show the flow from pond b to c. Illumination from the SW.

isolated enclaves and/or at the base of crater walls (e.g., 'S' in Figure S2), and are likely a consequence of late-stage deposition of debris-poor melt from the crater walls and central peak after emplacement of the main hummocky deposit [*Hawke and Head*, 1977; *Cintala and Grieve*, 1998; *Howard and Wilshire*, 1975; *Simonds et al.*, 1976]. Melt ponds are also sourced from adjacent topographically higher ponds [*Howard and Wilshire*, 1975], often through distinct channels (e.g., from pond 'a' to 'b' in Figure 1).

[7] Post-emplacement melt drainage is evidenced by the existence of strand-lines at pond edges [*Howard and Wilshire*, 1975] (Figures 2b and 2c), and collapsed melt pond crusts ('b' in Figure 1). The chaotic appearance of pond 'b' on the floor of Giordano Bruno crater (Figure S1a) suggests that pond-to-pond transfer occurred after the formation of a solid crust, creating a void beneath; the unsupported crust then partially collapsed creating a chaotic terrain. Shadow measurements to the deepest regions of the

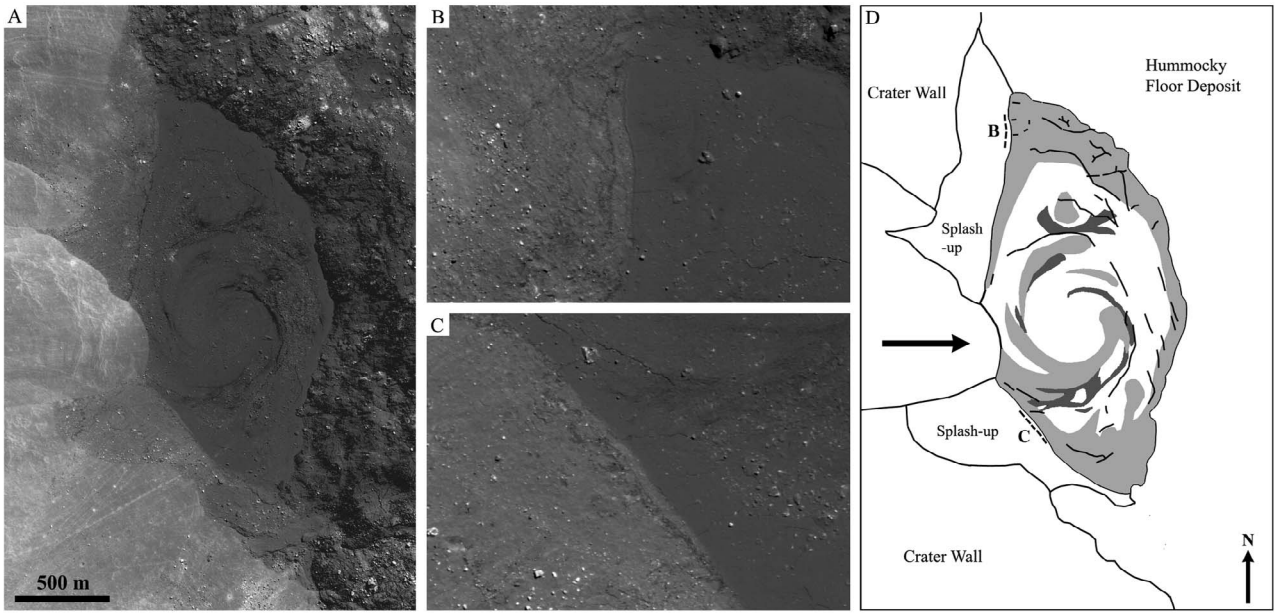

Figure 2. (a) LROC-NAC image M110919730R shows a melt pond in Giordano Bruno. (b and c) Strand-lines at the edges of the melt pond in Figure 2a. (Each 500 meters wide.) (d) Sketch map of Figure 2a. Strand-lines (dotted lines) occur along the crater wall. The pond surface has a spiral of smooth (light gray) and rougher (dark gray and unshaded) areas that are interpreted to be more debris rich. Prominent fractures are marked with black lines. Arrow marks the slump direction of material from the crater wall. Illumination from NE.

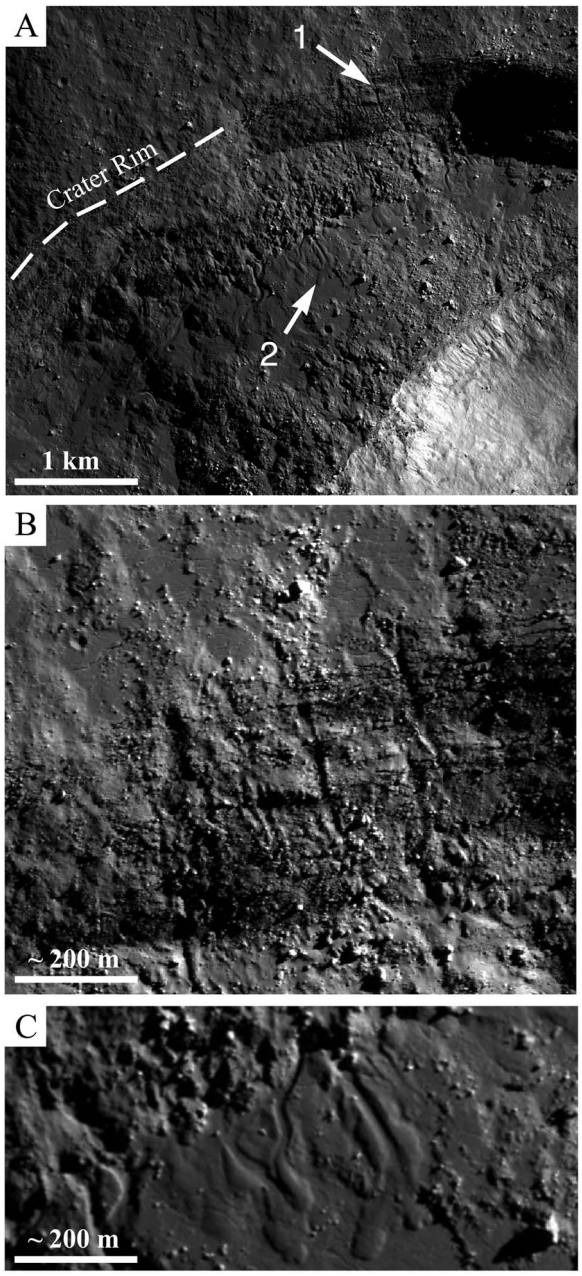

Figure 3. Portions of LROC image M104182009L. (a) Flows of impact melt on the SE slump block of Thales. (b and c) Here '1' and '2' from Figure 3a mark incised channels on the steep crater wall and leveed channels on the slump block surface, respectively. North is down, illumination from ENE.

pool (Figure S3) suggest a void depth up to ~110 m. Assuming this depth estimate is representative of the entire collapsed area, ~5 × 10^6 m^3 of melt drained from 'b' after the crust solidified. Measurements of rotated block thicknesses (assuming that originally horizontal surface blocks rotated to a vertical position) suggest that post-emplacement drainage to pond 'c' or into underlying breccia occurred after a crust ~8 m thick solidified on pond 'b'. We estimate it would take on the order of 2–5 years for this crust to form, assuming cooling by thermal radiation alone. Entrainment of large volumes of cold material could result in more rapid cooling of the melt [*Onorato et al.*, 1976; *Simonds et al.*, 1976]. For example, more than 15–20% cold debris in the melt would cause significant cooling (simulated by changing the initial temperature from 2000 K to 1600 K in our model); cold debris content of 50% would cause solidification in a matter of minutes.

[8] Figure 2a shows the source pond 'a' for the intra-pond flows in Figure 1, which exhibits a distinctive spiraled surface pattern of debris entrained or superimposed on an otherwise smooth crust. The spiral pattern and the relative paucity of visible fractures at the pond center indicate circulation after the formation of a crust that was still able to deform in a ductile manner. The circulation was likely initiated by influx of material from the crater walls (Figure 2d). Pond circulation is also evident in the larger hummocky melt sheet of Moore F (Figure S1b), where curved cracks (~50 m wide and up to ~1400 m in length) and flow lineations indicate large-scale movement around the central peak (Figure S2).

3.2. Erosion of Crater Walls by Impact Melt

[9] Ponds behind slump blocks and outside of the crater rim-crest are relatively smooth compared to hummocky floor deposits. The source of some near-rim flows can be identified as specific melt ponds close to the crater rim-crest, or topographic depressions – perhaps marking a drained source pond. Flows range from channeled to broader, apparently more viscous flow segments that exhibit decameter-scale ropy pahoehoe-like folds; both morphologies can occur within the same flow, typically with the relatively thin incised channel sections occurring closer to the flow source (Figure 3b) and terminating at broad single- or multi-lobe distal margins (Figure 3c).

[10] Figure 3a shows small (10s to 100s m across) ponds on Thales crater rim (Figure S1c), apparently feeding melt flows on the crater wall and slump block surface. Incised channels on the steep crater wall ('1' in Figure 3a) are ~20 m wide and indicate erosion of wall-rock (Figure 3b). On the lower gradient of the slump block surface, the incised channels transition to thickened flows with levees surrounding relatively well-defined channels (Figure 3c). The levees appear simpler than those formed by successive overbank deposits, and probably represent stabilization along the flow margins due to lateral flow gradients and cooling. The central channel was then formed by drainage of the central melt as the source was exhausted.

[11] Mechanical or thermal erosion of a substrate by turbulent lava requires a fast, low viscosity flow [e.g., *Hulme*, 1973]. Cooling by radiation and incorporation of cold debris increases viscosity of melt, preventing such erosion. Incised channels in Figure 3b show that after initial pooling in rim ponds, and incorporation of cold debris, the melt was still hot/fluid enough to erode the crater wall. This may be a consequence of the expected superheating of impact melts. Mechanical erosion by superheated impact melts thus provides an additional formation mechanism for gullies on impact crater walls that have been suggested to form via dry granular flow [*Bart*, 2007], or water in Martian examples [*Mellon and Phillips*, 2001]. Additionally, melt deposits already on the slump block may have formed a hot layer upon which the descending melt could easily flow without significant basal cooling, allowing a run out up to ~400 m onto the slump block.

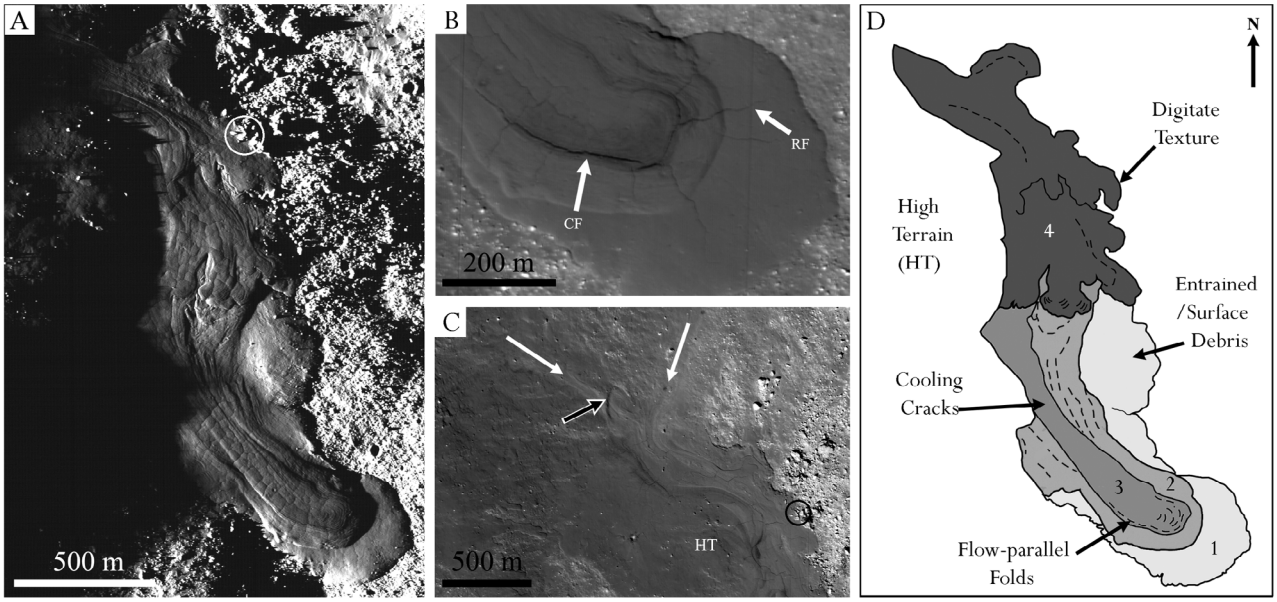

Figure 4. (a) Low sun image (M101476840L) of a flow outside the rim-crest of Giordano Bruno. Illumination from the west. (b) High sun image (M106209806R) of the flow-front, highlighting radial fractures (RF) and circumferential fractures (CF). Illumination from SW. (c) Flows of impact melt (white arrows) that merge to feed the main flow in Figure 4a. HT and the black-in-white arrow mark high terrain that influenced the path of the melt flow. Circles on Figures 4a and 4c mark the same boulder outcrop. (d) Sketch map of the flow section in Figure 4a. Flow sections are marked and shaded individually. Example locations of features noted in the text are marked with arrows.

3.3. Flow Inflation and Multiple Episodes of Melt Injection

[12] An external melt flow with diverse surface textures (Figure 4a) is sourced from an extensive (~5 × 5 km) melt deposit near the southern rim of Giordano Bruno. The flow has four distinct topo-stratigraphic sections (Figure 4d). Heights were calculated from shadow length measurements and have an error of ±11 cm (scaled pixel width of M101476840L is 1.515 m).

[13] The basal section ('1') is ~2 m thick and ~445 m wide at the flow front (Figure 4b), and has a simple morphology compared to terrestrial lava flows of similar breadth. This simplicity may be due to the wider source region, compared to a discrete vent of a typical terrestrial lava flow. Section '1' shows entrained or partially buried rocky debris at its edges. Flow sections '2' and '3' are ~6.5 and 8 m above section '1' respectively and display ductile flow lineations and/or folds parallel to the flow margins. The folds were most likely formed perpendicular to the flow direction, and then pushed outward by continued melt injection to form the elongate "flow-parallel" folds currently observed, similar to processes observed at channeled pahoehoe breakouts on Earth [*Gregg and Keszthelyi*, 2004]. The continuity of the folds indicates that this section of the flow advanced as a single 'simple' flow, rather than a 'compound' flow of coalesced breakouts.

[14] Circumferential fissures ('CF') up to ~5 m wide along the upper margins and orthogonal fractures on the surface of '2' and '3' resemble inflation fractures and adjacent cooling joints in terrestrial lava flows [*Hon et al.*, 1994]. This suggests that sections '2' and '3' formed through flow inflation driven by continued influx of melt, which built up behind the cooling flow front. Radial tearing fractures ('RF') emanating away from the circumferential inflation fractures crosscut both the top of the inflated flow (sections '2' and '3') and the basal sections ('1'), implying that these sections of the flow represent a single cooling unit. The fissures ('CF') in the inflated portion of the flow would have enhanced cooling of this region [*Walker*, 1991], perhaps explaining the absence of lobate breakouts at the front of the inflated section 2. This may have also prompted the later inflation episode, leading to an additional 1–2 m of inflation (section '3'). The tip of section '3' is slightly depressed (Figure S4), indicating later volume loss, perhaps by melt drainage or escape of a gas phase.

[15] The restriction of inflation to the center of the flow suggests the interior of section '1' was viscous enough to prevent injection of the later melt which formed inflated section '2'. Assuming cooling by thermal radiation, solidification of a 2 m thick flow would occur on the order of 2–3 weeks. Given the abrupt margins of inflated sections '2' and '3', and the several hundred m length of observed run-out distances of lunar flows elsewhere (e.g., Figure 3), in spite of likely incorporation of cooler rocky debris, we suggest that an extended hiatus in influx (days to weeks) may explain the morphology seen in Figure 4b.

[16] Closer to the flow source, a more complex, digitate flow morphology ('4') overlies the lower flow sections, representing a possible fourth stage of melt injection. The morphology of '4' is reminiscent of channel break-outs and multiple influx episodes of small volumes of melt noted in low effusion rate compound terrestrial pahoehoe flows [*Gregg and Keszthelyi*, 2004]. The late-stage influx of melt into the flow to form section '4' may thus have occurred at a slower emplacement rate than sections 1–3, possibly indicating gradual depletion of the source region and/or increasing melt viscosity.

[17] The apparent multi-pulse nature of the flow in Figure 4a requires staggered flux of melt into the cooling and shrinking molten core of the flow. Temporary ponding of melt in topographic lows further upslope and behind topographic obstacles (e.g., HT in Figures S4 and 4c), may have delayed the arrival of melt. Punctuated release of smaller melt volumes to create the digitate textures ('4') may be due to different melt ponds in the source region successively filling, coalescing, and over-flowing as melt continued to flow downslope and away from the crater rim. Seismic shaking produced by continued collapse of the crater interior may also facilitate disturbance of the melt in these ponds.

4. Conclusions

[18] The distribution and meter-scale morphology of impact melts in fresh complex lunar craters revealed in high-resolution LROC-NAC images provide evidence for multiple and extended episodes of melt remobilization after initial emplacement, and prior to complete solidification.

[19] Crater-fill deposits are comprised primarily of a mixture of melt and debris, overlain by a later-stage influx of relatively debris-poor melt forming smooth peripheral ponds (Figure S2). Fracture patterns on the surfaces of floor melt sheets preserve evidence of chaotic and even circulatory movements of the melt beneath a partially ductile crust. The longevity of movement in melt-bearing deposits has implications for possible melt sheet differentiation in large impact basins, as circulation may complicate and delay differentiation if the motion is more than a transient phenomenon occurring during the initial formation of a crust.

[20] Our observations and cooling estimates reveal continued movement between melt ponds on the crater floor (Figure 1), and demonstrate that impact melts within impact craters on the lunar surface may remain mobile for an extended period after impact (section 3.1). The prolonged mobility of crater floor melts may be facilitated by the warmth of the underlying melt-bearing crater floor deposit. Further from the crater floor, the ability of impact melts to maintain a low viscosity after emplacement, ponding, erosion and incorporation of colder debris (Figure 3) supports the likely superheated and highly mobile nature of impact melts.

[21] External melt deposits (Figure 4) show evidence of flow inflation and multiple episodes of ponding that suggest later melt remobilization can occur for up to 2–3 weeks. Solidification times between a few minutes to several years are physically possible, depending on the ratio of hot melt and cold clasts. The complex flow history revealed by the new LROC images argues against the shortest cooling times, although the opposite extreme of years is also unlikely. Further research is needed to determine if the melt was mobile for hours or months. Nevertheless, despite the almost instantaneous nature of impact melt generation and initial emplacement, we conclude that impact melts in and around craters are compound deposits created by multiple stages of flow.

[22] **Acknowledgments.** We gratefully acknowledge the Lunar Reconnaissance Orbiter Camera Team for discussions prior to and during the preparation of this manuscript. We thank Tracy K. P. Gregg and two anonymous reviewers for their constructive comments. This work was supported by the LRO Project.

References

Bart, G. D. (2007), Comparison of small lunar landslides and Martian gullies, *Icarus*, *187*, 417–421, doi:10.1016/j.icarus.2006.11.004.

Butler, P. (1973), Lunar sample information catalog: Apollo 17, *NASA MSC 03211*, Lunar Receiv. Lab., Houston, Tex.

Cintala, M. J., and R. A. F. Grieve (1998), Scaling impact-melt and crater dimensions: Implications for the lunar cratering record, *Meteoritics*, *33*, 889–912, doi:10.1111/j.1945-5100.1998.tb01695.x.

Gregg, T. K. P., and L. P. Keszthelyi (2004), The emplacement of pahoehoe toes: Field observations and comparison to laboratory simulations, *Bull. Volcanol.*, *666*, 381–391.

Hawke, B. R., and J. W. Head (1977), Impact melt on lunar crater rims, in *Impact and Explosion Cratering*, edited by D. J. Roddy et al., pp. 815–841, Pergamon, New York.

Hon, K., et al. (1994), Emplacement and inflation of pahoehoe sheet flows: Observations and measurements of active lava flows on Kilauea Volcano, Hawaii, *Geol. Soc. Am. Bull.*, *106*, 351–370, doi:10.1130/0016-7606(1994)106<0351:EAIOPS>2.3.CO;2.

Howard, K. A., and H. G. Wilshire (1975), Flows of impact melt at lunar craters, *J. Res. U.S. Geol. Surv.*, *3*, 237–251.

Hulme, G. (1973), Turbulent lava flow and the formation of lunar sinuous rilles, *Mod. Geol.*, *4*, 107–117.

Keszthelyi, L. P., and R. Denlinger (1996), The initial cooling of pahoehoe lave flow lobes, *Bull. Volcanol.*, *58*, 5–18, doi:10.1007/s004450050121.

Kieffer, S. W., and C. H. Simonds (1980), The role of volatiles and lithology in the impact cratering process, *Rev. Geophys.*, *18*, 143–181, doi:10.1029/RG018i001p00143.

Mellon, M. T., and R. J. Phillips (2001), Recent gullies on Mars and the source of liquid water, *J. Geophys. Res.*, *106*, 23,165–23,179, doi:10.1029/2000JE001424.

O'Keefe, J. D., and T. J. Ahrens (1975), Shock effects from a large impact on the moon, *Proc. Lunar Sci. Conf.*, *6th*, 2831–2844.

Onorato, P. I. K., D. R. Yhlmann, and C. H. Simonds (1976), Heat flow in impact melts: Apollo 17 Station 6 Boulder and some applications to other breccia and xenolith laden melts, *Proc. Lunar. Sci. Conf.*, *7th*, 2449–2467.

Pierazzo, E., and H. J. Melosh (2000), Melt production in oblique impacts, *Icarus*, *145*, 252–261, doi:10.1006/icar.1999.6332.

Robinson, M. S., et al. (2010), Lunar Reconnaissance Orbiter Camera (LROC) instrument overview, *Space Sci. Rev.*, *150*, 81–124, doi:10.1007/s11214-010-9634-2.

Simonds, C. H., J. L. Warner, and W. C. Phinney (1976), Thermal regimes in cratered terrain with emphasis on the role of impact melt, *Am. Mineral.*, *61*, 569–577.

Walker, G. (1991), Structure and origin by injection of lava under surface crust of tumuli, "lava rises", "lave-rise pits", and "lava-inflation clefts" in Hawaii, *Bull. Volcanol.*, *53*, 546–558, doi:10.1007/BF00298155.

V. J. Bray, C. M. Caudill, A. S. McEwen, B. Rizk, and L. L. Tornabene, Lunar and Planetary Laboratory, University of Arizona, Tucson, AZ 85721, USA. (vjbray@lpl.arizona.edu)

L. R. Gaddis and L. P. Keszthelyi, United States Geological Survey, 2255 North Gemini Dr., Flagstaff, AZ 86001, USA.

W. B. Garry, Center for Earth and Planetary Studies, National Air and Space Museum, Smithsonian Institution, Washington, DC 20024, USA.

T. A. Giguere and B. R. Hawke, Hawaii Institute of Geophysics and Planetology, University of Hawaii at Manoa, Honolulu, HI 96822, USA.

S. A. Kattenhorn, Department of Geological Sciences, University of Idaho, Moscow, ID 83843, USA.

C. H. van der Bogert, Institut für Planetologie, Westfälische Wilhelms-Universität, Münster, D-48149, Germany.